Liver Cirrhosis: Intravoxel Incoherent Motion MR Imaging—Pilot Study[1]

Alain Luciani, MD, PhD
Alexandre Vignaud, PhD
Madeleine Cavet, MD
Jeanne Tran Van Nhieu, MD
Ariane Mallat, MD, PhD
Lucile Ruel, PhD
Alexis Laurent, MD, PhD
Jean-François Deux, MD, PhD
Pierre Brugieres, MD
Alain Rahmouni, MD

Purpose: To retrospectively evaluate a respiratory-triggered diffusion-weighted (DW) magnetic resonance (MR) imaging sequence combined with parallel acquisition to allow the calculation of pure molecular-based (*D*) and perfusion-related (*D**, *f*) diffusion parameters, on the basis of the intravoxel incoherent motion (IVIM) theory, to determine if these parameters differ between patients with cirrhosis and patients without liver fibrosis.

Materials and Methods: The institutional review board approved this retrospective study; informed consent was waived. IVIM DW imaging was tested on three alkane phantoms, on which the signal-intensity decay curves according to *b* factors were logarithmically plotted. Ten *b* factors (0, 10, 20, 30, 50, 80, 100, 200, 400, 800 sec/mm^2) were used in patients. Patients with documented liver cirrhosis (cirrhotic liver group, $n = 12$) and patients without chronic liver disease (healthy liver group, $n = 25$) were included. The mean liver *D*, *D**, and *f* values were measured and compared with the apparent diffusion coefficient (ADC) computed by using four *b* values (0, 200, 400, 800 sec/mm^2). Liver ADC and *D*, *f*, and *D** parameters were compared between the cirrhotic liver group and healthy liver group. Means were compared by using the Student *t* test.

Results: Signal-intensity decay curves were monoexponential on phantoms and biexponential in patients. In vivo, mean ADC values were significantly higher than *D* in the healthy liver group (ADC = 1.39×10^{-3} mm^2/sec ± 0.2 [standard deviation] vs $D = 1.10 \times 10^{-3}$ mm^2/sec ± 0.7) and in the cirrhotic liver group (ADC = 1.23×10^{-3} mm^2/sec ± 0.4 vs $D = 1.19 \times 10^{-3}$ mm^2/sec ± 0.5) ($P = .03$). ADC and *D** were significantly reduced in the cirrhotic liver group compared with those in the healthy liver group (respective *P* values of .03 and .008).

Conclusion: Restricted diffusion observed in patients with cirrhosis may be related to *D** variations, which reflect decreased perfusion, as well as alterations in pure molecular water diffusion in cirrhotic livers.

[1] From the INSERM Unite U 841, Equipe 17, Molecular Mechanisms of Liver Fibrosis, Creteil, France (A. Luciani, J.T.V.N., A.M.); Departments of Radiology (A. Luciani, M.C., L.R., J.F.D., P.B., A.R.), Pathology (J.T.V.N.), Hepatology (A.M.), and Liver Surgery (A. Laurent), AP-HP, Groupe Henri Mondor Albert Chenevier, Centre Hospitalo Universitaire Henri Mondor, 51 Avenue du Marechal de Lattre de Tassigny, 94010 Creteil Cedex, France; and Siemens Medical Solutions France, Saint Denis, France (A.V.). Received January 12, 2008; revision requested April 2; revision received May 5; accepted June 12; final version accepted June 25. **Address correspondence to** A.L. (e-mail: *alain.luciani@hmn.aphp.fr*).

Radiology

Prior studies (1–12) have shown that liver fibrosis is associated with progressive restriction of diffusion motion and have suggested that this is probably because of the increase in connective tissue associated with liver fibrosis. By using diffusion-weighted (DW) magnetic resonance (MR) imaging and four distinct *b* values (0, 200, 400, and 800 sec/mm^2), a noninvasive diagnosis of severe fibrosis can be made with respective sensitivity, specificity, positive predictive value, and negative predictive value of 87%, 87%, 72%, and 94% when liver biopsy data are used as the reference standard (2). Intravoxel incoherent motion (IVIM) imaging is a method initially developed by Le Bihan et al (13) to quantitatively assess the microscopic translational motions that occur in each image voxel at MR imaging. Le Bihan et al (13,14) have demonstrated that both pure molecular diffusion and microcirculation, or blood perfusion, can be distinguished by using IVIM-based DW imaging, provided that multiple *b* values to encompass both low *b* values (<200 sec/mm^2) and high *b* values (>200 sec/mm^2) are used.

Advances in Knowledge

- Intravoxel incoherent motion (IVIM) diffusion-weighted (DW) imaging, which is a combination of parallel and respiratory-triggered acquisition, allows the extraction of pure molecular diffusion parameters (*D*) and perfusion-related diffusion parameters (*D**, *f*) within the liver parenchyma.
- Liver signal decay with a IVIM DW imaging sequence follows a biexponential curve, which accounts for a double component of liver diffusion—presumably, pure molecular diffusion and perfusion-related diffusion.
- Restricted global diffusion with decreased apparent diffusion coefficient observed in liver cirrhosis may be explained by a reduced *D** value, which reflects decreased liver perfusion.

Previously, the use of IVIM DW imaging has been limited to neuroradiologic applications because the abdominal organs can be subject to respiratory or motion artifacts, especially when long echo times are used (11). The advent of respiratory triggering combined with the use of parallel imaging reconstruction, however, caused us to wonder if IVIM DW imaging could be applied in the evaluation of the liver in patients with cirrhosis because blood perfusion in chronic liver disease is an important surrogate marker for the importance of liver fibrosis, as demonstrated with perfusion imaging studies (15–17).

The purpose of this study was to retrospectively evaluate a respiratory-triggered DW imaging sequence combined with parallel acquisition to allow the calculation of pure molecular-based (*D*) and perfusion-related (*D**, *f*) diffusion parameters, on the basis of the IVIM theory, to determine if these parameters differ between patients with cirrhosis and patients without liver fibrosis.

Materials and Methods

IVIM DW Imaging Sequence Design and Phantom Study

The IVIM DW imaging sequence was developed and applied with a 1.5-T MR imaging system (Avanto; Siemens, Erlangen, Germany) with Super Quantum (Siemens) gradients (maximum gradient amplitude of 40 mT/m, maximal gradient slope of 200 mT/m) and 18 channels (total imaging matrix system). The IVIM DW imaging sequence was implemented with developmental software (IDEA; Siemens). The sequence was based on standard single-shot DW spin echo-planar imaging, with multiple *b* values ranging from 10 sec/mm^2 to a maximum of 800 sec/mm^2. The minimal incremental value between two successive *b* values was set at 10 sec/mm^2, instead of the 50-sec/mm^2 interval authorized by the MR imager manufacturer.

Three distinct alkane phantoms were used to validate the IVIM DW imaging sequence in vitro. These phantoms consisted of either tridecane, pentadecane, or hexadecane. The phantoms differ from one another with regard to their alkyl chain lengths, which led to different, but precisely known, apparent diffusion coefficient (ADC) values (18). All corresponded to monocompartmental models of diffusion (18).

The three phantoms were imaged by using a body-array surface coil combined with one spine-array surface coil at a fixed MR imaging room temperature (22°C). The IVIM DW imaging sequence is detailed in Table 1. The calculation of the ADC for each phantom was performed by using Equation (1), where S_b is the signal intensity for each *b* value and S_0 is the signal intensity at a *b* value of zero:

$$\ln(S_b) = \ln(S_0) - b\mathrm{ADC}. \qquad (1)$$

ADC maps for each phantom were

Implication for Patient Care

- Unenhanced IVIM DW imaging enables the extraction of diffusion parameters reflecting microcirculation, or perfusion, within the liver parenchyma, which potentially could be used as surrogate markers for liver cirrhosis.

Published online
10.1148/radiol.2493080080

Radiology 2008; 249:891–899

Abbreviations:
ADC = apparent diffusion coefficient
DW = diffusion weighted
IVIM = intravoxel incoherent motion
ROI = region of interest

Author contributions:
Guarantors of integrity of entire study, A.L., A.R.; study concepts/study design or data acquisition or data analysis/interpretation, all authors; manuscript drafting or manuscript revision for important intellectual content, all authors; manuscript final version approval, all authors; literature research, A.L., M.C., J.T.V.N., L.R.; clinical studies, A.L., A.V., M.C., J.T.V.N., A.M., L.R., A.L.; experimental studies, A.L., A.V., L.R., P.B.; statistical analysis, A.L., A.R.; and manuscript editing, A.L., A.V., M.C., J.F.D., P.B., A.R.

See Materials and Methods for pertinent disclosures.

See also the editorial by Le Bihan in this issue.

hence generated. A rectangular region of interest (ROI) was placed by one of the authors (P.B., with 20 years of experience in MR imaging) within the center of each test liquid to avoid potential edge artifacts. The in-plane ROI for each measurement was 4 cm^2.

The performance of the IVIM DW imaging sequence was repeated three times for each phantom, thus providing three ADC values for each phantom that were averaged to provide the mean ADC value for each phantom.

Pilot Patient Study Design

Our study was approved by our Institutional Review Board at Centre Hospitalo Universitaire Henri Mondor, and the requirement for informed consent was waived. Technical support was endorsed by a Siemens employee (A.V.) for IVIM DW imaging sequence modifications and implementation with our MR imaging device. The authors not associated with Siemens maintained full control of the data at all times.

Inclusion criteria.—In November 2006, the IVIM DW imaging sequence was added to our routine liver MR imaging protocol. The files of 287 consecutive patients referred to our department between November 2006 and May 2007 for liver MR imaging were reviewed: Collected clinical data included age, sex, and history of alcohol abuse; collected laboratory data included serum aspartate aminotransferase level and platelet count; collected pathologic data consisted of liver biopsy findings obtained less than 2 months prior to liver MR imaging, including liver fibrosis assessment according to METAVIR score (19); additionally, transient elastography findings were also collected if obtained less than 2 months prior to liver MR imaging, with mean liver stiffness expressed in kilopascals (20). Both inclusion and exclusion criteria are provided in Table 2. Patients were included in either the cirrhotic liver group or in the healthy liver group.

All liver MR imaging examination findings in the included patients were reviewed by two radiologists (A. Luciani and A.R., with 10 and 20 years of experience, respectively, in abdominal MR imaging). Both radiologists in consensus looked for MR imaging signs of chronic liver disease, including nodularity and atrophy (23,24), liver steatosis on MR images, and the presence of hepatocellular carcinoma (25).

Study population.—Among the 287 patients who underwent liver MR imaging with IVIM DW imaging during the study period, a total of 250 patients were excluded: Among patients eligible for the healthy liver group, 77 patients with fatty liver at MR imaging and/or with missing laboratory findings were excluded. Among patients eligible for the cirrhotic liver group, 173 were excluded because of missing liver biopsy findings and/or because of pathologic findings consistent with a METAVIR score below F4. As a result, 37 patients were included in the final study population. These included 25 patients in the healthy liver group (12 men, 13 women) and 12 in the cirrhotic liver group (seven men, five women). Mean age in the healthy liver group was 48 years ± 16 (standard deviation) (range, 34–62 years), while mean age in the cirrhotic liver group was 55 years ± 13 (range, 51–71 years). Mean age of female patients was 52 years ± 19 (range, 35–71 years), while mean age of male patients was 56 years ± 20 (range, 34–70 years). The indications for liver MR imaging in the study population were as follows: follow-up in patients with chronic liver disease with or that without the presence of a focal liver lesion at

Table 1

Sequence Parameters Used for Phantom and In Vivo Liver MR Studies

Sequence	Study Type	Repetition Time (msec)/Echo Time (msec)/Flip Angle (degrees)	No. of *b* Values	No. of Signals Acquired	Matrix	Field of View	Section Thickness (mm)	Bandwidth (Hz/pixel)	GRAPPA	Contrast Material Injection	Acquisition Time
IVIM DW imaging	Phantom	1500/79/NA	16*	3	51 × 128	100 × 250	5	1300	2	NA	3 min 46 sec
T1-weighted gradient-echo in- and out-of-phase	In vivo liver MR imaging	119/2.4–4.8/70	NA	1	256 × 192	300 × 260	5	470	2	No	58 sec
T2-weighted turbo spin-echo	In vivo liver MR imaging	2410/82/150	NA	2	320 × 160	300 × 270	5	260	2	No	1 min 19 sec
IVIM DW imaging	In vivo liver MR imaging	1500/70/NA	10†	3	138 × 138	300 × 250	5	1342	2	No	2 min 16 sec
3D gradient-echo VIBE	In vivo liver MR imaging	3.17/1.33/20	NA	1	256 × 220	310 × 250	3	560	NA	No/Yes‡	20 sec (repeated three times)

Note.—GRAPPA = generalized autocalibrating partially parallel acquisition, NA = not applicable, 3D = three-dimensional, VIBE = volumetric interpolated breath-hold examination.

* 16 *b* values: 0, 10, 20, 30, 40, 50, 60, 70, 80, 90, 100, 200, 400, 800, and 1000 sec/mm^2.

† 10 *b* values: 0, 10, 20, 30, 40, 50, 100, 200, 400, and 800 sec /mm^2.

‡ VIBE sequences were performed before and repeated three times at 20-second intervals after the dynamic bolus injection of gadolinium chelate.

ultrasonography in the 12 patients in the cirrhotic liver group and further evaluation of a previously detected benign focal liver lesion in the 25 patients of the healthy liver group.

Patients were included in the cirrhotic liver group on the basis of pathologic data ($n = 7$), transient elastography data ($n = 1$), or surrogate serum markers that suggested the presence of liver cirrhosis combined with MR imaging signs of chronic liver disease ($n = 4$). In eight (67%) of these 12 patients, chronic liver disease was attributed to alcohol intake, while chronic hepatitis C viral infection was documented in four (33%) patients. Seven of these 12 patients had a diagnosis of a focal lesion consistent with hepatocellular carcinoma at MR imaging.

Twenty-five patients were included in the healthy liver group—eight patients with liver cyst, seven with liver hemangioma, and 10 with focal nodular hyperplasia.

Liver MR Imaging

All MR imaging examinations were performed at our institution with the same 1.5-T MR imaging system (Avanto) used in the phantom study. The liver MR imaging protocol included transverse T1-weighted gradient-echo in- and out-of-phase and transverse T2-weighted turbo spin-echo sequences (Table 1). IVIM DW images were acquired prior to gadolinium chelate injection. The IVIM DW imaging sequence was respiratory gated by using a pneumatic belt, which resulted in an average repetition time of 1500 msec. Finally, a dynamic three-dimensional volumetric interpolated breath-hold T1-weighted sequence was repeated before and three times after the injection of a total of 0.2 mL per kilogram of body weight gadoteric acid (Dotarem; Guerbet, Aulnay, France) (Table 1).

IVIM DW Image Analysis

Diffusion parameters with the IVIM method.—In biologic tissues, IVIM includes microcirculation of blood in the capillary network, which is also called perfusion (14). The relation between signal variation and b factors with an IVIM-type sequence can be expressed by using Equation (2) (14):

$$\frac{S_b}{S_0} = (1 - f) \cdot \exp(-bD) + f \cdot \exp[-b(D + D^*)], \quad (2)$$

where S is the mean signal intensity, f is the fraction of the diffusion linked to microcirculation, D is the diffusion parameter representing pure molecular diffusion (slow component of diffusion), and D^* is the diffusion parameter representing incoherent microcirculation within the voxel (perfusion-related diffusion, or fast component of diffusion).

Considering that D^* is significantly greater than D (14), its influence on signal decay can be neglected for b factors greater than 200 sec/mm^2. Equation (2) can then be simplified, and the estimation of D can be obtained by using only b values greater than 200 sec/mm^2, with a simple linear fit equation (3):

$$\frac{S_b}{S_0} = \exp(-bD). \quad (3)$$

With the D value determined by using Equation (3), f and D^* values can be calculated by using a nonlinear regression algorithm based on Equation (2), following the function description provided by Lagarias et al (26). When the function failed to converge, pixel values were automatically discarded. Overall, and in both the cirrhotic liver group and the healthy liver group, the number of excluded pixels never exceeded 0.5% of all liver pixels.

All regression algorithms were implemented with software (MatLab; Mathworks, Natick, Mass), which allowed the extraction of parametric maps representing f, D, and D^* parameters, which were fitted on a pixel-by-pixel basis.

ROI positioning and extraction of diffusion parameters.—All ROIs were manually positioned by two authors (A. Luciani and A.R.) on parametric maps obtained with software (MatLab). ROIs were positioned to avoid large vessels or liver segments with focal lesions identified on IVIM DW images acquired with a b factor of 0 sec/mm^2. The confirmation of the absence of a liver lesion or of a large vessel was provided by visually comparing the ROI positioning on IVIM DW images and on native T1-weighted and T2-weighted images. Two ROIs were positioned in the right liver lobe,

Table 2

Inclusion and Exclusion Criteria for 287 Patients Who Underwent Liver IVIM DW Imaging

Patient Group	Criteria
Cirrhotic liver group ($n = 12$)*	METAVIR F4 score at liver biopsy (19) performed within the past 2 months
	Mean liver stiffness at transient elastography >12.5 kPa (20, 21)
	APRI test result >2 associated with MR imaging signs of chronic liver disease (22)
Healthy liver group ($n = 25$)†	Negative HBV and HCV findings for chronic viral infection
	APRI test result <0.5
	No MR imaging signs of chronic liver disease, HCC, or fatty liver
	No evidence of liver fibrosis at liver biopsy performed within the past 2 months, if available
Excluded from study ($n = 250$)	Fatty liver at MR imaging or missing pathologic or biologic data which cannot allow correct classification of patients ($n = 77$)
	METAVIR score at liver biopsy below F4 in patients not eligible for healthy liver group ($n = 173$)

Note.—APRI was computed according to the following equation: APRI = aspartate aminotransferase (upper limit of normal) · 100/platelet count. (Platelet count in 10^9 cells per liter.) APRI = aspartate aminotransferase–to-platelet ratio index, HBV = hepatitis B virus, HCC = hepatocellular carcinoma, HCV = hepatitis C virus.

* For the cirrhotic liver group, only one of these criteria had to be met.

† For the healthy liver group, all of these criteria had to be met.

Table 3

Mean *D*, *D, and *f* Parameters Measured in Right and Left Lobe on a Per-Patient Basis**

Parameter	Healthy Liver Group			Cirrhotic Liver Group			Overall		
	Right Lobe	Left Lobe	*P* Value	Right Lobe	Left Lobe	*P* Value	Right Lobe	Left Lobe	*P* Value
D ($\times 10^{-3}$ mm^2/sec)	1.16 ± 0.9	1.02 ± 0.4	.5	1.27 ± 0.5	1.04 ± 0.6	.15	1.25 ± 0.5	1.02 ± 0.2	.24
*D** ($\times 10^{-3}$ mm^2/sec)	85.1 ± 27	71.0 ± 31	.1	57.4 ± 21	64.7 ± 26	.34	74.1 ± 21	69.4 ± 16	.31
f	0.26 ± 0.07	0.31 ± 0.09	.07	0.31 ± 0.09	0.29 ± 0.07	.76	0.29 ± 0.5	0.31 ± 0.6	.25

Note.—Data are means ± standard deviations. Mean right lobe measurements were obtained by averaging the parametric measurements obtained by using two right lobe ROIs. No significant differences were observed between lobes.

and one ROI was positioned in the left liver lobe. The mean size of all ROIs was 12 pixels ± 3, with a range from 10 to 16 pixels. The mean size of ROIs in the cirrhotic liver group and the healthy liver group were 13 pixels ± 2 and 12 pixels ± 4, respectively. For each ROI, the mean value of each parameter (*f*, *D*, and *D**) derived from the pixel-by-pixel analysis was computed. Mean values of *f*, *D*, and *D** obtained by averaging both right liver lobe ROI measurements were named f_R, D_R, and D^*_R. The values of *f*, *D*, and *D** obtained from the left liver lobe ROI measurement were named f_L, L_L, and D_L. Mean *D*, *f*, and *D** values obtained on a per-patient basis were obtained by averaging the three measurements (ie, the two right lobe measurements and the left lobe measurement).

A third diffusion coefficient, called global diffusion coefficient (ADC value), was obtained by using only *b* factors of 0, 200, 400, and 800 sec/mm^2 and was fitted to Equation (1). By using this postprocessing method and only four *b* factors, this value reflects the ADC values usually referenced in the literature (2). Three ROIs within each liver were positioned as detailed above on parametric ADC maps. Mean ADC values were obtained by averaging the three ADC values collected.

Statistical Analysis

Means were compared by using the Student *t* test. Right and left lobe measurements were compared by using a paired *t* test. For correlations between quantitative variables, we used the Pearson coefficient. $P < .05$ was considered to indicate a statistically significant difference. All statistical analyses were conducted by using software (SPSS, version 12.0 for Windows; SPSS, Chicago, Ill).

Results

Phantom Study

IVIM DW imaging signal showed a monoexponential decay with increasing *b* values for each phantom. The mean ADC values computed with all *b* factors for tridecane, hexadecane, and pentadecane phantoms were 6.77×10^{-4} mm^2/sec ± 0.19, 3.50×10^{-4} mm^2/sec ± 0.39, and 4.61×10^{-4} mm^2/sec ± 0.27, respectively.

Pilot Patient Study and IVIM DW Image Analysis

Among all patients, there was no significant difference between *D*, *D**, and *f* values obtained from the right or the left liver lobe (Table 3).

All curves of signal-intensity decrease demonstrated a biexponential-type decay as expected, whether the measurements were obtained in the healthy liver group or in the cirrhotic liver group (Figs 1, 2).

ADC values were significantly higher than *D* values, both in the healthy liver group and in the cirrhotic liver group ($P = .03$) (Table 4). Both ADC and *D** were significantly reduced in the cirrhotic liver group compared with those in the healthy liver group. There was no significant difference between *D* and *f* measurements in the healthy liver and the cirrhotic liver groups.

Discussion

Our findings confirm that liver diffusion combines both pure molecular diffusion (slow component of diffusion) and capillary perfusion (fast component of diffusion) (11). In our phantom study, the signal decay with the IVIM DW imaging sequence was monoexponential, thus suggesting that the biexponential signal decay encountered in vivo cannot be attributed to a systematic error based on our sequence design (27).

In vivo, our findings show that the liver diffusion component linked to perfusion (*D**) significantly decreased in the cirrhotic liver group compared with that in the healthy liver group and could account for the reduced ADC in cirrhotic livers reported in previous studies (1,2,6–8,11,12,28). Although most of these studies of DW imaging involved a small number of *b* values, with *b* values generally higher than 200 sec/mm^2, we believe that two mechanisms in liver fibrosis could have resulted in this overall reduced ADC:

1. Liver fibrosis is associated with progressive increase in connective tissue. Hence, the increased proportion of collagen fibers is believed to impair brownian water motion within fibrotic livers, thus leading to reduced ADC values. The global liver ADC values we obtained by selecting only four *b* factors were similar to those in previously published data (2). For instance, ADC values in the healthy liver group in our study were 1.39×10^{-3} mm^2/sec compared with 1.44×10^{-3} mm^2/sec in the Lewin et al (2) study. Results of IVIM DW imaging, however, suggest that the diffusion component related to the molecular displacement (*D*) does not differ significantly between cirrhotic and healthy livers. Similar findings have already been reported by Yamada et al (11), who found that *D* was significantly

lower than ADC, thus suggesting that differences reported in ADC between patients with cirrhosis and healthy patients were mainly related to the perfusion component of liver diffusion. The fact that the pure molecular diffusion coefficient, *D,* was similar in both the healthy liver group and the cirrhotic liver group further suggests that when considering DW imaging in cirrhotic livers, changes in liver architecture may be of less importance than changes in liver perfusion.

2. It is well accepted that liver cirrhosis is associated with reduced liver perfusion: The increased arterial flow triggered by intrahepatic portal hypertension in liver fibrosis is insufficient to compensate for the reduced portal flow (29). For Moreno et al (29,30), the mean portal flow in healthy subjects was 20.9 mL/min/kg ± 4.1 as opposed to 6.5 mL/min/kg ± 5.6 in patients with cirrhosis. Similar findings have been documented noninvasively, especially with perfusion computed tomography (31, 32). This could explain the observed decay of D^* in cirrhotic livers. Therefore, the assessment of D^* may potentially be considered as a surrogate marker of capillary liver perfusion. As such, D^* could be thought of as an indirect perfusion marker, rather than a diffusion coefficient (33). Few prior studies have shown the ability of DW imaging to provide D^* data. Yamada et al (11) were the first to test IVIM DW imaging in abdominal organs, although D^* values were not provided. Our study had a number of differences from the study by Yamada et al. In that study, four *b* values were used—30, 300, 900, and 1100 sec/mm^2 (11). Moreover, the echo time was 123 msec as opposed to 79 msec in our study, thus leading to increased sensitivity to motion artifacts. Furthermore, reducing echo time values enabled reduced T2 dependence and a potential increase in signal-to-noise ratio at IVIM DW imaging. Additionally, the higher number of *b* values used in our study could account for differences in the D values we obtained compared with those reported by Yamada et al (0.76×10^{-3} mm^2/sec in normal liver in Yamada et al study vs 1.1×10^{-3} mm^2/sec in our study). This hypothesis remains to be confirmed, as an exact comparison between IVIM sequences in previously published studies and our IVIM DW imaging sequences is difficult, especially regarding D^* calculations.

Interestingly, although D^* was significantly lower in the cirrhotic liver group than in the healthy liver group, our results suggest that the vascular volume fraction f was similar in both the cirrhotic liver group and the healthy liver group, as previously reported (11). It is, to date, difficult to provide a definite explanation for these apparent discrepancies. Although blood volume is reduced in liver cirrhosis (34), hepatic arterial vasodilatation occurs in response to reduced portal venous blood flow (35) and could explain the differences in terms of D^* and f variations.

Figure 1

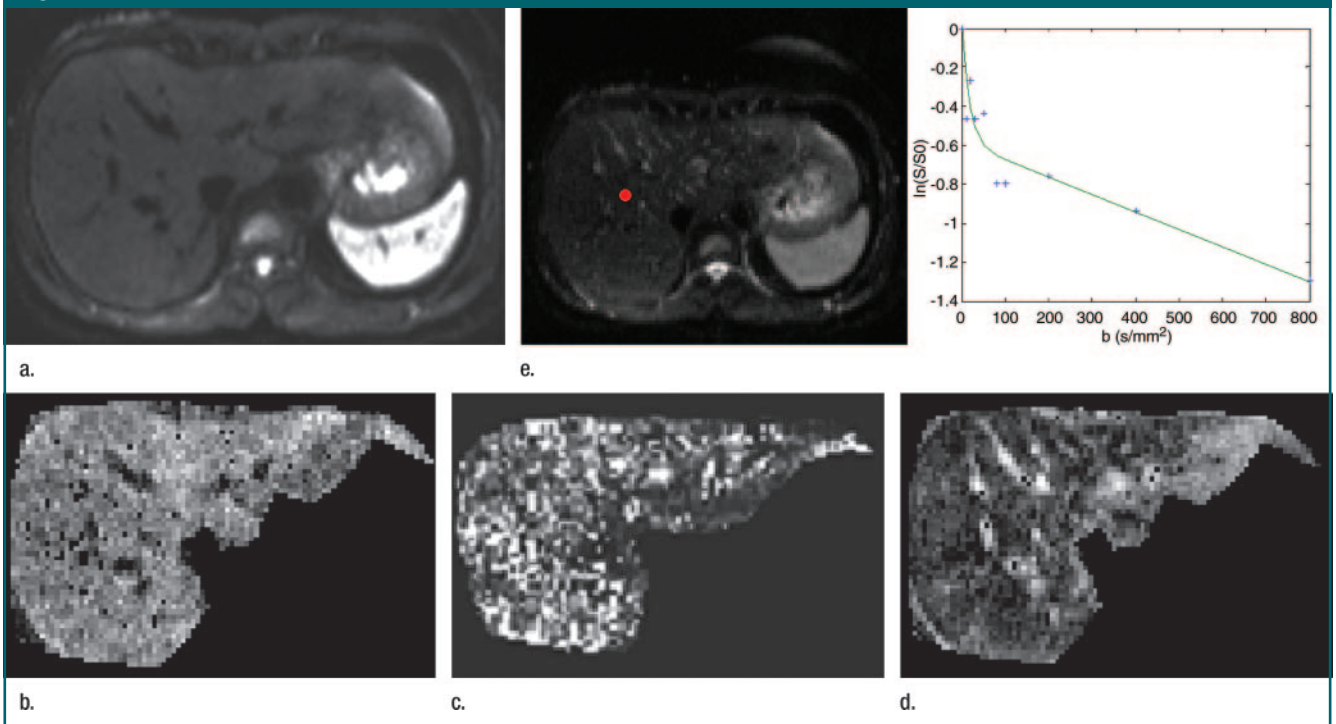

Figure 1: **(a–d)** IVIM DW images in 34-year-old woman referred to our department for the confirmation of a focal nodular hyperplasia diagnosis (lesion not shown). Patient was included in the healthy liver group. **(a)** Both native images were obtained with *b* value of 50 sec/mm^2. Parametric images allowed representation of **(b)** D, **(c)** D^*, and **(d)** f parameters. **(e)** Logarithmic plot of biexponential signal decay observed with a single-pixel measurement. Red dot = sole pixel.

Figure 2

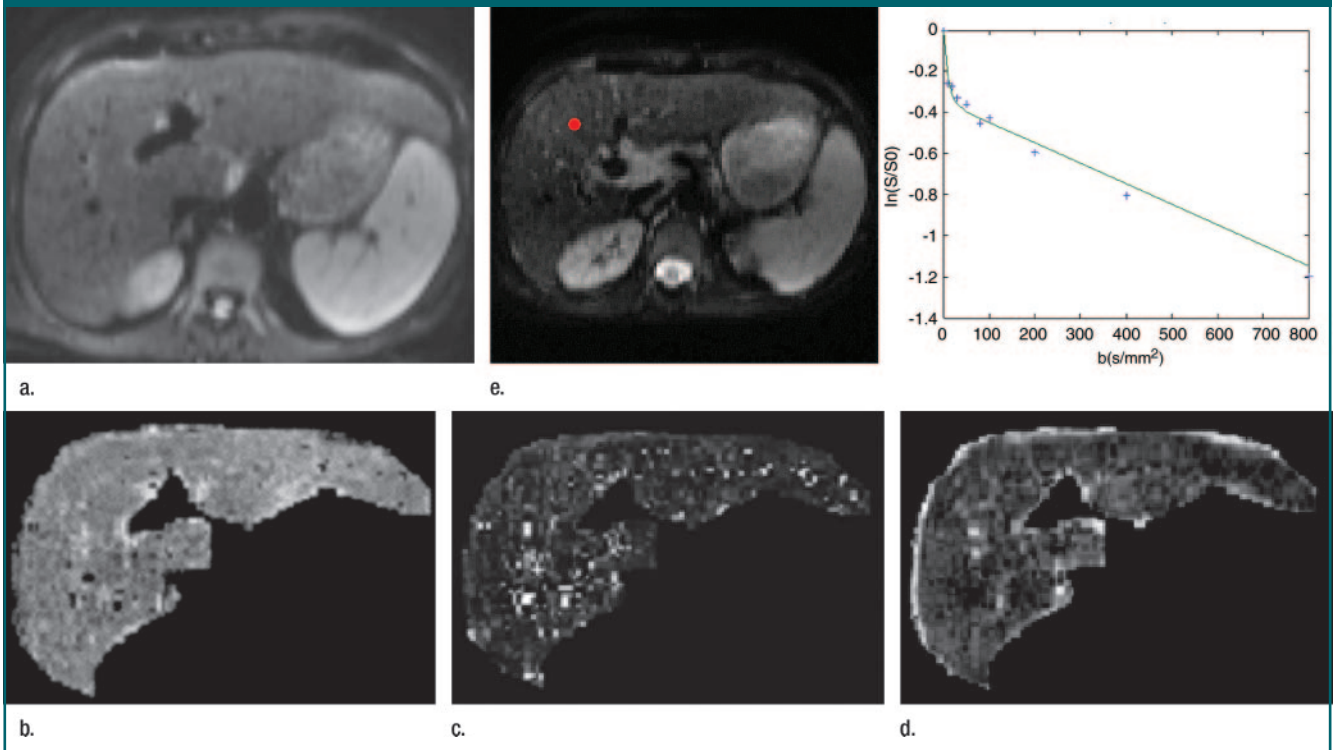

Figure 2: **(a–d)** IVIM DW images in 52-year-old woman referred to our department for suspicion of hepatocellular carcinoma and with biopsy-proved liver cirrhosis (hepatocellular carcinoma lesion not shown). Patient was included in the cirrhotic liver group. **(a)** Both native images were obtained with *b* value of 50 sec/mm^2. Parametric images allow representation of **(b)** *D*, **(c)** *D**, and **(d)** *f* parameters. **(e)** Logarithmic plot of biexponential signal decay observed with a single-pixel measurement. Initial slope of the signal-intensity decay is reduced compared with what was observed in healthy liver group, which was consistent with decreased *D**. Red dot = sole pixel.

Both *D** and *f* values could therefore reflect distinct perfusion properties.

Our study had several limitations. Imaging data from a large number of patients had to be excluded because of missing pertinent data required for study inclusion. As a result, only 37 patients were included in the study. The causes of chronic liver disease in the 12 patients in the cirrhotic liver group were heterogeneous, and histopathologic confirmation of liver cirrhosis was available in only seven of these 12 patients. However, the inclusion criteria we used for the healthy liver group were based on well-accepted noninvasive diagnostic criteria (22). Moreover, aspartate aminotransferase–to-platelet ratio index scores were always combined with MR imaging data as inclusion criteria. We acknowledge that this pilot study included only two distinct populations—those with cirrhotic livers and those with healthy livers. The ability of IVIM DW imaging to help provide a more subtle distinction, especially between patients with METAVIR scores of F0 and F1 and those with scores of F2 to F4, could not be assessed. Similarly, providing sensitivity and specificity values of IVIM DW imaging for diagnosis of liver cirrhosis was beyond the scope of this study. Animal studies involving IVIM DW imaging are currently under way at our institution to provide more precise information on the relationship between the degree of fibrosis and *D** values.

Table 4

Mean global ADC and *D*, *D, and *f* Parameters Assessed in 37 Patients in Pilot Study**

Parameter	Healthy Liver Group	Cirrhotic Liver Group	*P* Value
ADC ($\times 10^{-3}$ mm^2/sec)	1.39 ± 0.2	1.23 ± 0.4	.03
D ($\times 10^{-3}$ mm^2/sec)	1.10 ± 0.7	1.19 ± 0.5	.4 (NS)
*D** ($\times 10^{-3}$ mm^2/sec)	79.1 ± 18.1	59.4 ± 20.0	.008
f (%)	27.0 ± 5.3	30.0 ± 5.7	.07 (NS)

Note.—Data are means ± standard deviations. NS = not significant.

In this pilot study, ROIs were manually positioned on parametric images extracted with software (MatLab). Because our aim was to avoid large vessels and liver segments with focal lesions, the size of ROIs was therefore limited. This probably limited the effect of benign or malignant liver lesions on diffu-

sion measurements, especially *D** measurements, both in the cirrhotic liver and healthy liver groups. However, the ROI size limitation could be overcome with greater confidence if ROIs could be positioned on anatomic images and automatically projected on parametric images. However, because the diffusion calculations used in this study were performed on a pixel-by-pixel basis, we believe that the diffusion measurements obtained in a homogeneous region of the liver should not be affected by the size of the ROI itself.

In our pilot study, simultaneous assessment of liver perfusion MR imaging was impossible owing to the study design: All patients were referred to our institution for suspicion of having focal liver lesion and thus required conventional liver MR imaging protocol. Combining perfusion MR imaging with IVIM DW imaging was therefore beyond the scope of our study.

In conclusion, the data collected from the 37 patients in our study confirm that the signal decay observed with increasing *b* factors by using IVIM DW imaging follows a biexponential pattern. Our findings confirm that *D* values (pure molecular diffusion), although lower than ADC values, do not differ significantly between healthy and cirrhotic livers (36). Our results further suggest that the ADC reduction observed in cirrhotic livers could be linked to decreased *D** values and may be related to reduced perfusion in cirrhotic livers.

Acknowledgments: The authors thank the MR imaging team at Centre Hospitalo Universitaire Henri Mondor, especially Pierre Zerbib, for their contribution to MR imaging experiments.

References

1. Taouli B, Tolia AJ, Losada M, et al. Diffusion-weighted MRI for quantification of liver fibrosis: preliminary experience. AJR Am J Roentgenol 2007;189:799–806.
2. Lewin M, Poujol-Robert A, Boelle PY, et al. Diffusion-weighted magnetic resonance imaging for the assessment of fibrosis in chronic hepatitis C. Hepatology 2007;46:658–665.
3. Bruegel M, Holzapfel K, Gaa J, et al. Characterization of focal liver lesions by ADC measurements using a respiratory triggered diffusion-weighted single-shot echo-planar MR imaging technique. Eur Radiol 2008;18:477–485.
4. Nasu K, Kuroki Y, Sekiguchi R, Kazama T, Nakajima H. Measurement of the apparent diffusion coefficient in the liver: is it a reliable index for hepatic disease diagnosis? Radiat Med 2006;24:438–444.
5. Koinuma M, Ohashi I, Hanafusa K, Shibuya H. Apparent diffusion coefficient measurements with diffusion-weighted magnetic resonance imaging for evaluation of hepatic fibrosis. J Magn Reson Imaging 2005;22:80–85.
6. Taouli B, Martin AJ, Qayyum A, et al. Parallel imaging and diffusion tensor imaging for diffusion-weighted MRI of the liver: preliminary experience in healthy volunteers. AJR Am J Roentgenol 2004;183:677–680.
7. Taouli B, Vilgrain V, Dumont E, Daire JL, Fan B, Menu Y. Evaluation of liver diffusion isotropy and characterization of focal hepatic lesions with two single-shot echo-planar MR imaging sequences: prospective study in 66 patients. Radiology 2003;226:71–78.
8. Boulanger Y, Amara M, Lepanto L, et al. Diffusion-weighted MR imaging of the liver of hepatitis C patients. NMR Biomed 2003;16:132–136.
9. Murtz P, Flacke S, Traber F, van den Brink JS, Gieseke J, Schild HH. Abdomen: diffusion-weighted MR imaging with pulse-triggered single-shot sequences. Radiology 2002;224:258–264.
10. Moteki T, Horikoshi H, Oya N, Aoki J, Endo K. Evaluation of hepatic lesions and hepatic parenchyma using diffusion-weighted reordered turboFLASH magnetic resonance images. J Magn Reson Imaging 2002;15:564–572.
11. Yamada I, Aung W, Himeno Y, Nakagawa T, Shibuya H. Diffusion coefficients in abdominal organs and hepatic lesions: evaluation with intravoxel incoherent motion echo-planar MR imaging. Radiology 1999;210:617–623.
12. Ichikawa T, Haradome H, Hachiya J, Nitatori T, Araki T. Diffusion-weighted MR imaging with single-shot echo-planar imaging in the upper abdomen: preliminary clinical experience in 61 patients. Abdom Imaging 1999;24:456–461.
13. Le Bihan D, Breton E, Lallemand D, Aubin ML, Vignaud J, Laval-Jeantet M. Separation of diffusion and perfusion in intravoxel incoherent motion MR imaging. Radiology 1988;168:497–505.
14. Le Bihan D, Turner R, MacFall JR. Effects of intravoxel incoherent motions (IVIM) in steady-state free precession (SSFP) imaging: application to molecular diffusion imaging. Magn Reson Med 1989;10:324–337.
15. Hollingsworth KG, Lomas DJ. Influence of perfusion on hepatic MR diffusion measurement. NMR Biomed 2006;19:231–235.
16. Pandharipande PV, Krinsky GA, Rusinek H, Lee VS. Perfusion imaging of the liver: current challenges and future goals. Radiology 2005;234:661–673.
17. Fournier LS, Cuenod CA, de Bazelaire C, et al. Early modifications of hepatic perfusion measured by functional CT in a rat model of hepatocellular carcinoma using a blood pool contrast agent. Eur Radiol 2004;14:2125–2133.
18. Brugieres P, Thomas P, Maraval A, et al. Water diffusion compartmentation at high b values in ischemic human brain. AJNR Am J Neuroradiol 2004;25:692–698.
19. Bedossa P, Poynard T. An algorithm for the grading of activity in chronic hepatitis C. The METAVIR Cooperative Study Group. Hepatology 1996;24:289–293.
20. Castera L, Vergniol J, Foucher J, et al. Prospective comparison of transient elastography, Fibrotest, APRI, and liver biopsy for the assessment of fibrosis in chronic hepatitis C. Gastroenterology 2005;128:343–350.
21. Nguyen-Khac E, Capron D. Noninvasive diagnosis of liver fibrosis by ultrasonic transient elastography (Fibroscan). Eur J Gastroenterol Hepatol 2006;18:1321–1325.
22. Wai CT, Greenson JK, Fontana RJ, et al. A simple noninvasive index can predict both significant fibrosis and cirrhosis in patients with chronic hepatitis C. Hepatology 2003;38:518–526.
23. Awaya H, Mitchell DG, Kamishima T, Holland G, Ito K, Matsumoto T. Cirrhosis: modified caudate-right lobe ratio. Radiology 2002;224:769–774.
24. Mortele KJ, Ros PR. MR imaging in chronic hepatitis and cirrhosis. Semin Ultrasound CT MR 2002;23:79–100.
25. Llovet JM, Fuster J, Bruix J. The Barcelona approach: diagnosis, staging, and treatment of hepatocellular carcinoma. Liver Transpl 2004;10(S2):S115–S120.
26. Lagarias JC, Reeds JA, Wright MH, Wright PE. Convergence properties of the Nelder-Mead Simplex Method in Low Dimensions. SIAM J Optimization 1998;9:112–147.
27. Tofts PS, Lloyd D, Clark CA, et al. Test liquids for quantitative MRI measurements of self-diffusion coefficient in vivo. Magn Reson Med 2000;43:368–374.

28. Guan S, Zhou KR, Zhao WD, Peng WJ, Tang F, Mao J. Magnetic resonance diffusion-weighted imaging in the diagnosis of diffuse liver diseases in rats. Chin Med J (Engl) 2005;118:639–644.

29. Moreno AH, Burchell AR, Rousselot LM, Panke WF, Slafsky F, Burke JH. Portal blood flow in cirrhosis of the liver. J Clin Invest 1967;46:436–445.

30. Moreno AH, Rousselot LM, Panke WF, Burke ML. The rate of hepatic blood flow in normal subjects and in patients with portal hypertension. Surg Gynecol Obstet 1960; 111:443–450.

31. Van Beers BE, Leconte I, Materne R, Smith AM, Jamart J, Horsmans Y. Hepatic perfusion parameters in chronic liver disease: dynamic CT measurements correlated with disease severity. AJR Am J Roentgenol 2001; 176:667–673.

32. Hashimoto K, Murakami T, Dono K, et al. Assessment of the severity of liver disease and fibrotic change: the usefulness of hepatic CT perfusion imaging. Oncol Rep 2006;16: 677–683.

33. Le Bihan D, Turner R. The capillary network: a link between IVIM and classical perfusion. Magn Reson Med 1992;27:171–178.

34. Van Beers BE, Grandin C, Pauwels S, et al. Gd-EOB-DTPA enhancement pattern of hepatocellular carcinomas in rats: comparison with Tc-99m-IDA uptake. J Magn Reson Imaging 1994;4:351–354.

35. Zipprich A, Steudel N, Behrmann C, et al. Functional significance of hepatic arterial flow reserve in patients with cirrhosis. Hepatology 2003;37:385–392.

36. Yagyu Y, Awai K, Inoue M, et al. MDCT of hypervascular hepatocellular carcinomas: a prospective study using contrast materials with different iodine concentrations. AJR Am J Roentgenol 2005;184:1535–1540.